2017 American Control Conference
Sheraton Seattle Hotel
May 24–26, 2017, Seattle, USA

Evaluating performance of multivariable vibration isolators: A frequency domain identification approach applied to an industrial AVIS

Michiel Beijen[1], Marcel Heertjes[1,2], Robbert Voorhoeve[1], Tom Oomen[1]

Abstract— **Vibration isolation is essential for industrial high-precision systems in suppressing the influence of external disturbances. The aim of this paper is to develop an identification method to estimate the transmissibility matrix for such systems. The transmissibility matrix is a key performance indicator in vibration isolation, but its identification is severely limited by the heavy weight and size of many industrial systems. Two non-parametric system identification methods based on periodic and spectral analysis are compared. It is shown that spectral analysis can benefit from random floor excitations at low frequencies and periodic shaker excitations at high frequencies. Using this method, a transmissibility matrix between 1 and 100 Hz is successfully measured on an industrial active vibration isolation system (AVIS), demonstrating that the proposed method is suitable for identification of these heavy-weight systems.**

I. Introduction

Vibration isolators are widely used in high-precision systems (e.g. wafer scanners [1], scanning tunneling microscopes [2], [3], measurement systems [4], [5]) to isolate machinery from disturbances otherwise entering from the supporting structure or floor [6]. A well-known performance indicator for such isolators is the transmissibility function. For single-axis systems, the transmissibility function describes the transfer from base frame vibrations to payload vibrations. For multi-axis systems, the transmissibility function is extended to a transmissibility matrix, or a scalar function derived from this transmissibility matrix [7], [8].

An estimation of the transmissibility matrix can be obtained from experimental data by placing e.g. accelerometers or geophones on both the base frame and the isolated payload of the machine. In, e.g., [8], [9], several methods for transmissibility matrix measurements are developed where external shakers are used to ensure that the base frame is sufficiently excited. In this case, the measured base frame excitation can be considered as a noise-free input signal. This leads in general to an unbiased estimate of the transmissibility matrix with a low variance. However, these methods are often not applicable to high-precision machines with industrial vibration isolators, which are usually heavy-weight systems (in the order of several tons), i.e. too heavy for off-the-shelf shakers to support and excite the system.

Alternative identification methods using environmental vibrations, e.g., floor vibrations as base frame excitation do not need external shakers, given that these vibrations have sufficient input energy in relevant frequency ranges. However, since the excitations are not known beforehand and are generally non-periodic, available methods are restricted to those that can deal with random noise. Moreover, sensor noise on both the base frame and payload measurement leads to an error-in-variables identification problem [10], [11], which is well-known to lead to biased estimates [12], [13]. An example of transmissibility function estimation via floor vibrations is found in [14], where spectral analysis with Hanning windows is used to estimate the transmissibility function of a single air mount, but not for a complete machine. In [15] an estimation method is applied to a small-scale multi-axis vibration isolator that assumes the cross-correlation between all measured inputs to be zero, but this is often not the case for an industrial environment. In [16] a multivariable method is presented that uses principal component analysis to assess the quality of the measurement, but only uses simulation results for its validation.

Although vibration isolation is essential in high-tech equipment and a variety of control methods is present, at present their experimental comparison is hampered by the lack of a systematic performance identification approach. In this paper, such an approach is developed that builds upon standard frequency domain identification methods [17]. In particular, (a) periodic analysis, and (b) spectral analysis are considered. The main contribution of this paper is to obtain a frequency response function of the transmissibility matrix by combining system identification obtained through floor excitations (at the lower frequencies) with periodic shaker-induced excitations (at the higher frequencies). This approach is validated on an industrial vibration isolation setup in the (wafer scanner) relevant frequency range between 1–100 Hz.

The paper is organized as follows. Section II describes the experimental setup and the identification problem. The non-parametric estimation methods based on periodic and spectral analysis are summarized in Section III. The experimental results are presented in Section IV, and the major conclusions are given in Section V.

II. System description

The system used for evaluation of the transmissibility matrix is the Active Vibration Isolation System (AVIS) shown in Fig. 1. The AVIS consists of two main parts: (i) a movable payload of 290 kg, and (ii) a base frame that is supported by the floor. The payload and base frame are connected by four isolator modules. These isolator modules provide a low stiffness and damping through pneumatically controlled air mounts to obtain passive vibration isolation. Three out of four modules are equipped with accelerometers

[1]Department of Mechanical Engineering, Group of Control Systems Technology, Eindhoven University of Technology, 5600 MB Eindhoven, The Netherlands, contact: M.A.Beijen@tue.nl

[2]ASML, Mechatronic Systems Development, 5504 DR Veldhoven, The Netherlands

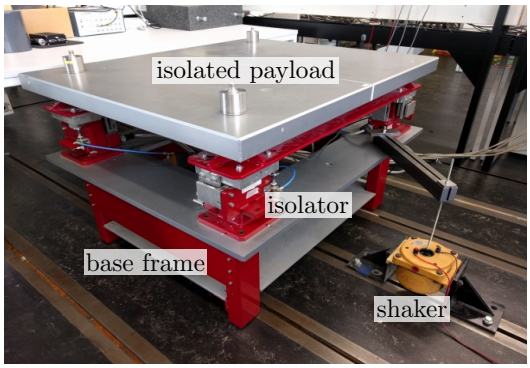

Fig. 1. AVIS used for validation of the transmissibility matrix measurements.

for measurement of the absolute payload acceleration in vertical direction denoted by $\ddot{\boldsymbol{q}}_{\mathbf{1}}(t) \in \mathbb{R}^3$. Furthermore, three accelerometers are attached to the base frame, measuring the base frame accelerations denoted by $\ddot{\boldsymbol{q}}_{\mathbf{0}}(t) \in \mathbb{R}^3$. Both $\ddot{\boldsymbol{q}}_{\mathbf{0}}$ and $\ddot{\boldsymbol{q}}_{\mathbf{1}}$ are filtered using a second-order high-pass filter at 0.1 Hz and a low-pass filter at 450 Hz to reduce sensor noise, cross-talk, and drift. Data acquisition is performed by a 16-bit real-time target running at 2 kHz. To apply base frame excitations in vertical direction, shakers are attached to three different locations on the base frame. For more information regarding the setup description, the reader is referred to [18], [19].

A. Coordinate transformation

For transmissibility matrices, it is common practice to define both the inputs and outputs with respect to a global coordinate system. Therefore, a coordinate transformation is performed to transform $\boldsymbol{q}_{\mathbf{0}}$ and $\boldsymbol{q}_{\mathbf{1}}$ to respectively $\boldsymbol{x}_{\mathbf{0}}(t) = [z_0, \theta_{x0}, \theta_{y0}]^T$ and $\boldsymbol{x}_{\mathbf{1}}(t) = [z_1, \theta_{x1}, \theta_{y1}]^T$. Herein, z indicates a vertical translation of the payload, and θ_x, θ_y indicate rotations around the two horizontal axes of the payload. Under the assumption of small displacements, the coordinate frames are related by

$$\boldsymbol{x}_{\mathbf{0}}(t) = \mathbf{R}_{\mathbf{0}}\boldsymbol{q}_{\mathbf{0}}(t), \quad \boldsymbol{x}_{\mathbf{1}}(t) = \mathbf{R}_{\mathbf{1}}\boldsymbol{q}_{\mathbf{1}}(t), \tag{1}$$

with transformation matrices $\mathbf{R}_{\mathbf{0}}, \mathbf{R}_{\mathbf{1}} \in \mathbb{R}^{3\times3}$.

B. Problem definition

The problem addressed in this paper is to find a frequency response function (FRF) of the transmissibility matrix $\mathcal{T}$, which is defined by the linear mapping

$$\boldsymbol{X}_{\mathbf{1}}(\omega) = \mathcal{T}(j\omega)\boldsymbol{X}_{\mathbf{0}}(\omega), \tag{2}$$

with $\boldsymbol{X}_{\mathbf{1}}(\omega), \boldsymbol{X}_{\mathbf{0}}(\omega)$ representing frequency-domain representations of the signals $\boldsymbol{x}_{\mathbf{1}}, \boldsymbol{x}_{\mathbf{0}}$. Since these signals are measured as sampled signals $\boldsymbol{x}_{\mathbf{1}}(kT_s), \boldsymbol{x}_{\mathbf{0}}(kT_s)$ having sampling time T_s and $k = 0, 1, ..., N-1$, the Discrete Fourier Transforms (DFT) of these signals will be used. As such, $\boldsymbol{X}_{\mathbf{1}}(\omega), \boldsymbol{X}_{\mathbf{0}}(\omega)$ are only considered at the N frequencies $\omega_k = (2\pi k)/(NT_s)$,

$$\boldsymbol{X}(\omega_k) = \frac{1}{\sqrt{N}} \sum_{n=0}^{N-1} \boldsymbol{x}(kT_s)e^{-j\omega_k nT_s}. \tag{3}$$

In the remainder of this paper, the abuse of notation $\omega \equiv \omega_k$ is used in the interest of compactness and readability.

Frequency-domain system identification techniques are used which need sufficient excitation power for $\boldsymbol{X}_{\mathbf{0}}$ (or its derivatives) in the frequency range of interest. The problem is, however, that it is difficult to sufficiently excite the base frame with shakers due to its heavy weight, in particular in the lower frequency range. Therefore, the following combination of excitation signals is proposed:

1. At low frequencies ($<$ 10 Hz), floor vibrations appear to have an average power of 10^{-9} $(\mathrm{m/s^2})^2/\mathrm{Hz}$, which is significantly above the noise level of the used accelerometers. This power will be used as excitation input for the base frame at low frequencies.
2. At high frequencies ($>$ 10 Hz), the excitation power from floor vibrations rapidly drops, but here it is possible to inject sufficiently strong excitation signals using off-the-shelf shakers.

It is expected that combining these two excitation sources leads to sufficient excitation power in the complete frequency range of interest, which is typically 1–100 Hz for industrial precision machines.

III. Non-parametric system identification

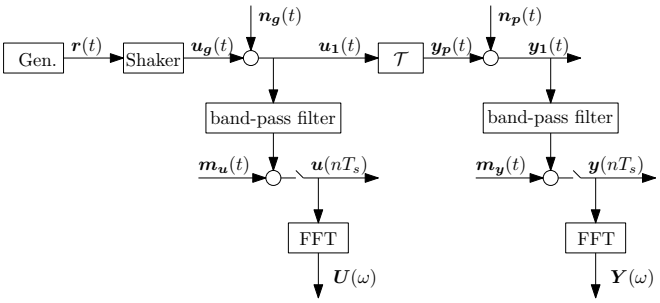

Fig. 2. Block diagram for non-parametric system identification methods.

Consider the block diagram in Fig. 2. In this block diagram, the transmissibility matrix is represented by the linear time-invariant transfer function $\mathcal{T}$ having base frame disturbances $\boldsymbol{u}_{\mathbf{1}}$ as input and resulting payload motions $\boldsymbol{y}_{\mathbf{1}}$ as output. Both $\boldsymbol{u}_{\mathbf{1}}$ and $\boldsymbol{y}_{\mathbf{1}}$ are estimated by the measurements $\boldsymbol{u} = \ddot{\boldsymbol{x}}_{\mathbf{0}}$ and $\boldsymbol{y} = \ddot{\boldsymbol{x}}_{\mathbf{1}}$, respectively, where the measurements contain additive measurement noise $\boldsymbol{m}_{\boldsymbol{u}}$ and $\boldsymbol{m}_{\boldsymbol{y}}$, respectively. Signal $\boldsymbol{u}_{\mathbf{1}}$ consists of two parts, namely $\boldsymbol{u}_{\boldsymbol{g}}$ containing the shaker-induced excitations, and $\boldsymbol{n}_{\boldsymbol{g}}$ containing the floor vibrations. The shaker block represents the transfer function from reference $\boldsymbol{r}$ to $\boldsymbol{u}_{\boldsymbol{g}}$. The output signal $\boldsymbol{y}_{\mathbf{1}}$ consists of $\boldsymbol{y}_{\boldsymbol{p}}$ representing payload accelerations due to base frame vibrations, and process noise $\boldsymbol{n}_{\boldsymbol{p}}$ representing payload accelerations due to direct payload disturbances (e.g. acoustic waves).

Two *direct* estimation approaches are presented in this section to address the identification problem. This means that estimation of $\mathcal{T}$ is based on measurement data of $\boldsymbol{u}$ and $\boldsymbol{y}$ only. An alternative is to use *indirect* methods, which also use data of $\boldsymbol{r}$ and therefore can provide unbiased estimates for $\mathcal{T}$ even if there is a significant contribution of noise. However, the drawback of indirect methods is that $\boldsymbol{r}$ must be known, which is infeasible if one wants to estimate the transmissibility matrix based on floor excitations. Therefore, indirect methods are not considered in this paper. For more information regarding the two direct methods, the reader is referred to [17].

A. Periodic analysis

To avoid leakage effects the input signal $\boldsymbol{U_0}$ is assumed to be N_p-periodic, and an integer number of periods M of the steady-state response is collected, giving $N = MN_p$ samples per experiment. By doing so, the measurement data of one experiment can be split into M periods which (ideally) contain identical data for $\boldsymbol{Y}, \boldsymbol{U}$ in every period. Neglecting transient effects, the measured output can be written in the frequency domain as

$$\boldsymbol{Y}(\omega) = \boldsymbol{Y_0}(\omega) + \boldsymbol{N_Y}(\omega), \tag{4}$$

with corresponding noise-free output

$$\boldsymbol{Y_0}(\omega) = \mathcal{T}(j\omega)\boldsymbol{U_0}(\omega), \quad \boldsymbol{U_0} = \boldsymbol{U_G}, \tag{5}$$

and output noise

$$\boldsymbol{N_Y}(\omega) = \boldsymbol{M_Y}(\omega) + \boldsymbol{N_P}(\omega) + \mathcal{T}(j\omega)\boldsymbol{N_G}(\omega). \tag{6}$$

Note that, although $\boldsymbol{N_G}$ can possibly provide useful information about $\mathcal{T}$, it is considered as noise in this method because it is generally non-periodic. Similar to $\boldsymbol{Y}$, the measured input $\boldsymbol{U}$ can be written as

$$\boldsymbol{U}(\omega) = \boldsymbol{U_G}(\omega) + \boldsymbol{N_U}(\omega), \tag{7}$$

with input noise

$$\boldsymbol{N_U}(\omega) = \boldsymbol{M_U}(\omega) + \boldsymbol{N_G}(\omega). \tag{8}$$

The following assumptions are introduced regarding the noise:

Assumption 1 (Disturbances)**.** *The noise signals $\boldsymbol{N_U}, \boldsymbol{N_Y}$ satisfy*

$$\begin{aligned}
&\mathbb{E}\left[\boldsymbol{N_U}(\omega)\right] = \boldsymbol{0}, \quad \mathbb{E}\left[\boldsymbol{N_Y}(\omega)\right] = \boldsymbol{0},\\
&\mathbb{E}\left[\boldsymbol{N_U}(\omega)\boldsymbol{N_U}^T(\omega)\right] = \boldsymbol{0}, \ \mathbb{E}\left[\boldsymbol{N_Y}(\omega)\boldsymbol{N_Y}^T(\omega)\right] = \boldsymbol{0},\\
&\mathbb{E}\left[\boldsymbol{N_Y}(\omega)\boldsymbol{N_U}^T(\omega)\right] = \boldsymbol{0},\\
&\mathbb{E}\left[\boldsymbol{N_U}(\omega)\boldsymbol{N_U}^H(\omega)\right] = \mathbf{C_U}(\omega),\\
&\mathbb{E}\left[\boldsymbol{N_Y}(\omega)\boldsymbol{N_Y}^H(\omega)\right] = \mathbf{C_Y}(\omega),\\
&\mathbb{E}\left[\boldsymbol{N_Y}(\omega)\boldsymbol{N_U}^H(\omega)\right] = \mathbf{C_{YU}}(\omega).
\end{aligned} \tag{9}$$

Assumption 2 (Disturbances - continued)**.** *The noise signals $\boldsymbol{N_U}, \boldsymbol{N_Y}$ are independent of the signals $\boldsymbol{U_0}, \boldsymbol{Y_0}$.*

The influence of noise can be reduced by averaging $\boldsymbol{Y}, \boldsymbol{U}$ over multiple periods. Define $\boldsymbol{Y}^{[i]\{l\}}$ as the l^{th} measured period in the i^{th} experiment. Under Assumptions 1 and 2,

$$\hat{\boldsymbol{Y}}_{\boldsymbol{0}}^{[i]}(\omega) = \frac{1}{M}\sum_{l=1}^{M}\boldsymbol{Y}^{[i]\{l\}}(\omega), \tag{10}$$

gives an unbiased estimate of $\boldsymbol{Y_0}$ in experiment $[i]$. By conducting as many independent experiments as inputs n_u, $i = 1, ..., n_u$, the following matrix is constructed:

$$\hat{\mathbf{Y}}_{\mathbf{mat}}(\omega) = \begin{bmatrix} \hat{\boldsymbol{Y}}_{\boldsymbol{0}}^{[1]}(\omega) & \hat{\boldsymbol{Y}}_{\boldsymbol{0}}^{[2]}(\omega) & ... & \hat{\boldsymbol{Y}}_{\boldsymbol{0}}^{[n_u]}(\omega) \end{bmatrix}. \tag{11}$$

Similar to (10) and (11), $\hat{\boldsymbol{U}}_{\boldsymbol{0}}^{[i]}$ and $\mathbf{U_{mat}}$ can be defined. Given periodic data, the input-output relation can be written as

$$\hat{\mathbf{Y}}_{\mathbf{mat}}(\omega) = \hat{\mathcal{T}}(j\omega)\hat{\mathbf{U}}_{\mathbf{mat}}(\omega). \tag{12}$$

Then, an estimate of the transmissibility matrix is given by

$$\hat{\mathcal{T}}(j\omega) = \hat{\mathbf{Y}}_{\mathbf{mat}}(\omega)\hat{\mathbf{U}}_{\mathbf{mat}}^{-1}(\omega). \tag{13}$$

for all frequencies ω where $\det(\hat{\mathbf{U}}_{\mathbf{mat}}(\omega)) \neq 0$.

Remark 3. *The condition* $\det(\hat{\mathbf{U}}_{\mathbf{mat}}(\omega)) \neq 0$ *ensures that* $\mathbf{U_{mat}}(\omega)$ *is invertible. This requires suitable experiment design, i.e. n_u independent experiments. To realize this, the reference $\boldsymbol{r}$ consists of random-phase multi-sine signals that are used to excite the base frame at different locations using shakers.*

1) Bias and variance: The signals $\boldsymbol{N_Y}, \boldsymbol{N_U}$ could lead to a non-zero bias and variance in $\hat{\mathcal{T}}$. Under Assumptions 1 and 2, it is derived in [17, Sec. 2.7] that the FRF estimate is asymptotically unbiased, i.e.

$$\text{a.s.}\lim_{M\to\infty}\hat{\mathcal{T}}(j\omega) = \mathcal{T}(j\omega), \tag{14}$$

and the covariance of the FRF [17, Sec. 2.7] is estimated as

$$\begin{aligned}
&\text{Cov}(\text{vec}(\hat{\mathcal{T}}(j\omega))) \approx (\overline{\hat{\mathbf{U}}_{\mathbf{mat}}(\omega)\hat{\mathbf{U}}_{\mathbf{mat}}^H(\omega)})^{-1}\otimes\\
&\qquad\qquad \left(\mathbf{V}(\omega)\hat{\mathbf{C}}_{\mathbf{z}}(\omega)\mathbf{V}^H(\omega)\right),\\
&\mathbf{V}(\omega) = [\mathbf{I}_{n_y} - \hat{\mathcal{T}}(j\omega)],\\
&\hat{\mathbf{C}}_{\mathbf{z}}(\omega) = \begin{bmatrix} \hat{\mathbf{C}}_{\mathbf{Y}}(\omega) & \hat{\mathbf{C}}_{\mathbf{YU}}(\omega) \\ \hat{\mathbf{C}}_{\mathbf{YU}}^H(\omega) & \hat{\mathbf{C}}_{\mathbf{U}}(\omega) \end{bmatrix}.
\end{aligned} \tag{15}$$

In (15), $\otimes$ is the Kronecker product, the overbar denotes a complex conjugate, and $\hat{\mathbf{C}}_{\mathbf{U}}(\omega)$, $\hat{\mathbf{C}}_{\mathbf{Y}}(\omega)$, and $\hat{\mathbf{C}}_{\mathbf{YU}}(\omega)$ are the input-output noise covariance matrices of one experiment (one column of $\hat{\mathbf{Y}}_{\mathbf{mat}}(\omega)$ and $\hat{\mathbf{U}}_{\mathbf{mat}}(\omega)$). For sufficient large M, and a good input signal-to-noise ratio (SNR), the covariance asymptotically decreases to zero [17]. An estimate for the covariance is given by

$$\begin{aligned}
\hat{\mathbf{C}}_{\mathbf{YU}}^{[i]}(\omega) = \frac{1}{M}\frac{1}{(M-1)}\sum_{l=1}^{M}&\left(\boldsymbol{Y}^{[i]\{l\}}(\omega) - \hat{\boldsymbol{Y}}_{\boldsymbol{0}}^{[i]}(\omega)\right)\\
&\left(\boldsymbol{U}^{[i]\{l\}}(\omega) - \hat{\boldsymbol{U}}_{\boldsymbol{0}}^{[i]}(\omega)\right)^H,
\end{aligned}$$

Note that in (15) it is assumed that $\hat{\mathbf{C}}_{\mathbf{Y}}^{[i]} = \hat{\mathbf{C}}_{\mathbf{Y}}$, $\hat{\mathbf{C}}_{\mathbf{U}}^{[i]} = \hat{\mathbf{C}}_{\mathbf{U}}$, $\hat{\mathbf{C}}_{\mathbf{YU}}^{[i]} = \hat{\mathbf{C}}_{\mathbf{YU}}$.

B. Spectral analysis

In this method, the measured output is written as

$$\boldsymbol{Y}(\omega) = \boldsymbol{Y_0}(\omega) + \boldsymbol{N_Y}(\omega), \tag{16}$$

with corresponding noise-free output

$$\boldsymbol{Y_0}(\omega) = \mathcal{T}(j\omega)\boldsymbol{U_0}(\omega), \tag{17}$$

having noise-free input $\boldsymbol{U_0}(\omega) = \boldsymbol{U_G}(\omega) + \boldsymbol{N_G}(\omega)$, and output noise

$$\boldsymbol{N_Y}(\omega) = \boldsymbol{M_Y}(\omega) + \boldsymbol{N_P}(\omega). \tag{18}$$

Note that, in contrast to periodic analysis in Section III-A, this method uses both $\boldsymbol{U_G}$ and $\boldsymbol{N_G}$ in $\mathbf{U_0}$, i.e. both signals provide useful information to estimate $\mathcal{T}$. The measured input $\boldsymbol{U}$ can be written as

$$\boldsymbol{U}(\omega) = \boldsymbol{U_G}(\omega) + \boldsymbol{N_U}(\omega), \tag{19}$$

with input noise $\boldsymbol{N_U}(\omega) = \boldsymbol{M_U}(\omega)$.

Using random excitations to identify multiple-input multiple-output (MIMO) systems, a full record of data $\boldsymbol{y}, \boldsymbol{u}$ is measured for a sufficiently long time. The full record is subsequently split into M subrecords of equal length denoted $\boldsymbol{y}^{[l]}$, $\boldsymbol{u}^{[l]}$ with $l = 1, ..., M$. Then, $\boldsymbol{y}^{[l]}$ and $\boldsymbol{u}^{[l]}$ are multiplied with a Hanning window to reduce the effects of leakage [17], and the DFTs $\boldsymbol{Y}^{[l]}(\omega)$ and $\boldsymbol{U}^{[l]}(\omega)$ are calculated for all l. Having calculated all $\boldsymbol{Y}^{[l]}(\omega)$ and $\boldsymbol{U}^{[l]}(\omega)$, estimates for the auto-spectrum matrix $\hat{\mathbf{S}}_{\mathbf{UU}}(\omega) \in \mathbb{C}^{n_u \times n_u}$ and cross-spectrum matrix $\hat{\mathbf{S}}_{\mathbf{YU}}(\omega) \in \mathbb{C}^{n_u \times n_u}$ are obtained by averaging over the M blocks, i.e.

$$\hat{\mathbf{S}}_{\mathbf{YU}}(\omega) = \frac{1}{M}\sum_{l=1}^{M} \boldsymbol{Y}^{[l]}(\omega)(\boldsymbol{U}^{[l]}(\omega))^H, \tag{20}$$

$$\hat{\mathbf{S}}_{\mathbf{UU}}(\omega) = \frac{1}{M}\sum_{l=1}^{M} \boldsymbol{U}^{[l]}(\omega)(\boldsymbol{U}^{[l]}(\omega))^H. \tag{21}$$

The so-called H_1 estimator for $\mathcal{T}$ can be defined (see e.g. [17], [20], [21]):

$$\hat{\mathcal{T}}(j\omega) = \hat{\mathbf{S}}_{\mathbf{YU}}(\omega)\hat{\mathbf{S}}_{\mathbf{UU}}^{-1}(\omega). \tag{22}$$

The H_1 estimator is a good choice when the output noise on $\boldsymbol{y}$ is large compared to the input noise on $\boldsymbol{u}$. When there is no output noise but significant input noise, the H_2 estimator should be used [21]. When there is both input and output noise, and there is a priori knowledge about the noise spectra, more advanced estimators can be defined that result in less bias, see e.g. [16]. However, in the context of vibration isolation, it is fair to assume that the SNR of $\boldsymbol{u}$ is much better than the SNR of $\boldsymbol{y}$, at least beyond the suspension frequency where isolation occurs. Therefore, it makes sense to use the H_1 estimator in this context.

1) Bias and variance: An expression for the FRF estimate using the H_1 estimator is derived in Appendix A, and reads

$$\begin{aligned}\hat{\mathcal{T}}(j\omega) \approx \left(\mathbf{I} + \mathbf{C}_{\mathbf{YU}}(\omega)(\mathbb{E}[\boldsymbol{Y_0}(\omega)\boldsymbol{U_0}^H(\omega)])^{-1}\right)\mathcal{T}(j\omega) \\ \left(\mathbf{I} + \mathbf{C}_{\mathbf{U}}(\omega)(\mathbb{E}[\mathbf{U_0}(\omega)\mathbf{U_0}^H(\omega)])^{-1}\right)^{-1}.\end{aligned} \tag{23}$$

Eq. (23) shows that the FRF estimate is unbiased if the input noise is zero. However, if there is input noise such that $\mathbf{C}_{\mathbf{U}} \neq \mathbf{0}$, (23) shows that bias appears.

An estimate for the covariance of $\hat{\mathcal{T}}$ is given by [17, Sec. 7.2.3]

$$\text{Cov}(\text{vec}(\hat{\mathcal{T}}(j\omega))) = \frac{1}{M}(\mathbf{S}_{\mathbf{UU}}^{-1}(\omega))^T \otimes \hat{\mathbf{C}}_{\mathbf{Y}}(\omega) \tag{24}$$

where the output noise covariance is estimated as

$$\hat{\mathbf{C}}_{\mathbf{Y}}(\omega) = \frac{M}{q}\left(\hat{\mathbf{S}}_{\mathbf{YY}}(\omega) - \hat{\mathbf{S}}_{\mathbf{YU}}(\omega)\hat{\mathbf{S}}_{\mathbf{UU}}^{-1}(\omega)\hat{\mathbf{S}}_{\mathbf{YU}}^{H}(\omega)\right), \tag{25}$$

with $q = M - n_u$ the number of the degrees of freedom in the residual.

Remark 4. *The estimates* (23) *for bias, and* (24) *for the covariance, might become inaccurate due to input noise. This is because the H_1 estimator assumes that the input noise is zero. This assumption is necessary to estimate the output noise covariance as in* (25) *in this direct identification method.*

IV. Experimental results

Identification experiments are presented in this section to estimate the transmissibility matrix. Bode plots are used to show $\hat{\mathcal{T}}$, and $\sigma(\hat{\mathcal{T}})$ which denotes the standard deviation of $\hat{\mathcal{T}}$. Expressions for $\hat{\mathcal{T}}$ are given in (13) and (22) for periodic and spectral analysis, respectively. Expressions for $\sigma(\hat{\mathcal{T}})$ are obtained by taking the square roots of the variances as defined in (15) and (24) for periodic and spectral analysis, respectively.

For ease of presentation, and given the fact that the floor mostly provides vibrations in Z-direction, This section only presents measurement results for this direction. The following measurement sets are analyzed in the subsections:

(A) Shaker excitation is turned off, so the base frame is only excited by floor vibrations. Since there is no periodic excitation, this measurement set is only analyzed using spectral analysis.

(B) The shaker provides a periodic multi-sine signal with a length of 10 s. The grid of excited frequencies ranges from 10 to 100 Hz with a resolution of 0.1 Hz. All excited frequencies have equal power. Periodic analysis is used, which means that floor excitations will be averaged out from the data.

(C) The same data as in (B) is used but now spectral analysis is applied. By doing so, both floor and shaker excitations are considered as useful excitation source.

All measurement sets have a total measurement time of six minutes. To prevent drift of the sensor signals during measuring, analogue high-pass filters are applied at 0.1 Hz

for the accelerometers, recall Section II. The power spectral densities in Z-direction for all measurement sets are shown in Fig. 3. This figure clearly shows the benefit of combining the excitation power from the floor and the shakers. The power from the floor rapidly drops for frequencies beyond 10 Hz, while the shakers only provide reasonable high-frequency excitation due to the positive slope of the spectral plot.

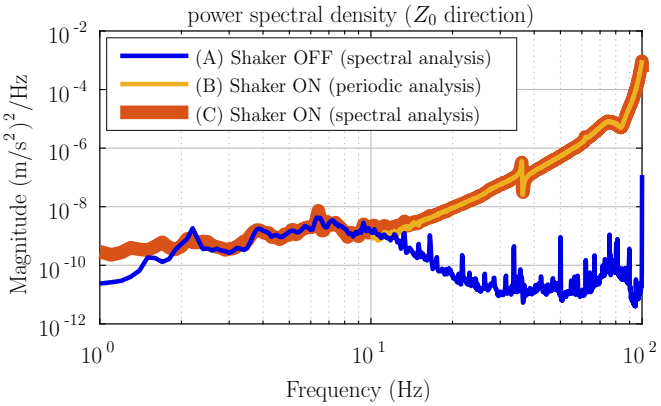

Fig. 3. Measured power spectral density plots on the base frame in Z_0-direction. Note that spectral analysis with shaker ON combines floor excitations at low frequencies with shaker excitations at high frequencies, leading to good excitation conditions from 1–100 Hz.

A. Measurement with only floor excitations

In this measurement, a data sequence of $\boldsymbol{u}$ and $\boldsymbol{y}$ is recorded for six minutes. The measurement sequence is split in 36 subrecords of 10 seconds each, to which spectral analysis (Section III-B) is applied. To compensate for data loss due to windowing, a 67% overlap factor is used. Fig. 4(a) shows the estimated transmissibility function in Z-direction. At low frequencies, the magnitude converges to 0 dB, which is as expected because below the suspension frequency the base frame and payload behave as a single rigid-body having the same motion in the same coordinate frame. Furthermore, two suspension modes are visible around 3-4 Hz. The FRF shows a desired roll-off until 20 Hz, clearly showing the benefit of vibration isolation. Beyond 20 Hz, both the FRF and the standard deviation suddenly increase. This is due to the fact that the excitation power from the floor is low with respect to the sensor noise level, see Fig. 3, leading to a poor SNR. As a consequence, the plot is believed to be inaccurate beyond 20 Hz in view of Remark 4.

B. Measurement with floor and shaker excitations (periodic analysis)

In this measurement, the base frame is excited three times 150 seconds using shakers that are attached to three different locations on the base frame. This leads to three times 15 periods with a length of 10 s having identical multi-sine shaker excitation inputs. To reduce transient effects, the first three periods of each experiment are discarded. Apart from periodic shaker excitations, random floor vibrations will also excite the base frame, but these excitations are considered as random noise in periodic analysis. Assuming that the shaker excitations are dominant, see Fig. 3 for the validity of this assumption, three independent experiments are performed, recall Remark 3. Using periodic analysis (Section III-A), the random floor vibrations are considered as undesired noise that should be removed from the measurement data by averaging over the periods. The resulting FRF and its standard deviation are shown in Fig. 4(B). The relatively high standard deviation at frequencies below 30 Hz illustrates a high uncertainty in the measurements. For frequencies beyond 30 Hz the standard deviation becomes significantly lower than the estimated FRF such that for high frequencies the FRF estimate is assumed to be accurate.

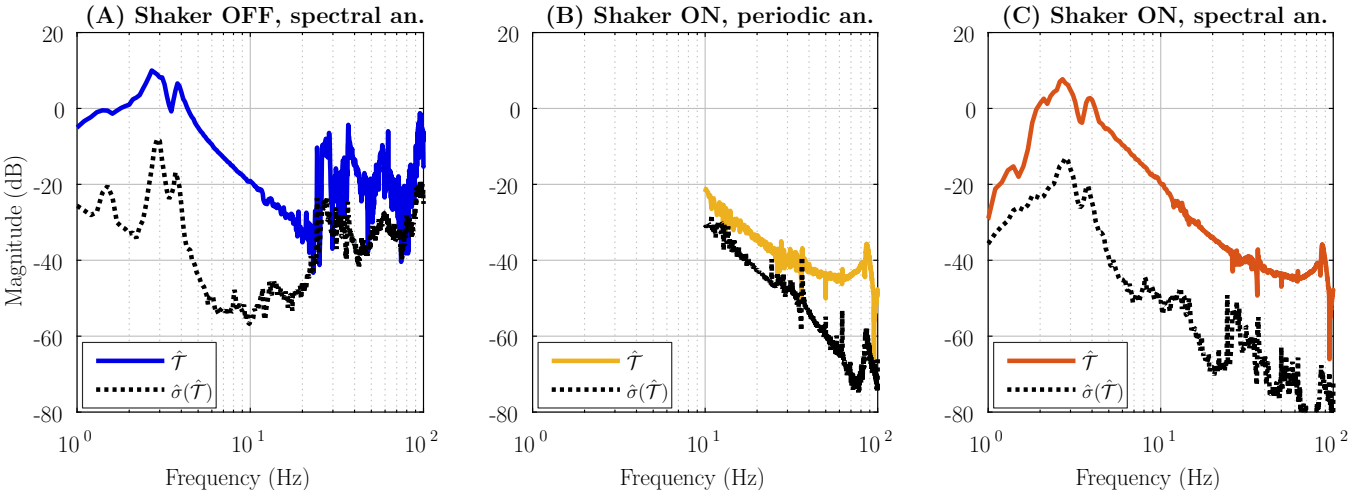

Fig. 4. Bode magnitude plots of the estimated transmissibility function ($\hat{T}$, blue/yellow/red), and corresponding standard deviation ($\sigma(\hat{T})$, black) for the measurements (A) without shaker excitation and spectral analysis, (B) with shaker excitation and periodic analysis, and (C) with shaker excitation and spectral analysis. In plot (A), the standard deviation might be inaccurate beyond 20 Hz in view of Remark 4. Plot (B) only shows results from 10–100 Hz because this is the range of excited frequencies in the multi-sine signal provided to the shaker. Plot (C) gives the best results, because it combines floor excitation at low frequencies with shaker excitations at high frequencies.

C. Measurement with floor and shaker excitations (spectral analysis)

Using the measurement data from Section IV-B for spectral analysis (Section III-B), both shaker and floor vibrations are treated as useful excitation input for the base frame. Similar to (A), the data is split into sub-records of 10 seconds each, and an overlap factor of 67% is used. The results are shown in Fig. 4(C). Comparing this figure to the results in Figs. 4(A,B), it follows that this approach nicely combines the benefits of floor excitations at low frequencies and shaker excitations at high frequencies, thus estimating the transmissibility function for the complete frequency range from 1 to 100 Hz. However, compared to (A), the plot of $\hat{\mathcal{T}}$ in (C) does not longer converge to 0 dB below the suspension mode due to shaker-induced noise at very low frequencies (< 2 Hz) , see Fig. 3.

V. Conclusions

Non-parametric identification methods based on periodic analysis and spectral analysis are used to estimate the transmissibility matrix of an industrial vibration isolator from different measurement sets. The measurements without shaker excitation can only provide a good FRF estimate for the Z_0 input direction at low frequencies. The measurements with shaker excitation and periodic analysis can provide reliable measurements for frequencies >10 Hz. For lower frequencies, the shaker is unable to sufficiently excite the base frame. The measurement with shaker excitation and spectral analysis combines the advantages of both excitation sources, leading to a good non-parametric identification in the complete frequency range.

References

[1] M. Heertjes, I. Sahin, N. van de Wouw, and W. Heemels, "Switching control in vibration isolation systems," *IEEE Transactions on Control Systems Technology*, vol. 21, no. 3, pp. 626–635, 2013.

[2] K. Iwaya, R. Shimizu, T. Hashizume, and T. Hitosugi, "Systematic analyses of vibration noise of a vibration isolation system for high-resolution scanning tunneling microscopes," *Review of Scientific Instruments*, vol. 82, no. 8, p. 083702, 2011.

[3] S. Ito, D. Neyer, S. Pirker, J. Steininger, and G. Schitter, "Atomic force microscopy using voice coil actuators for vibration isolation," in *2015 IEEE International Conference on Advanced Intelligent Mechatronics (AIM)*. IEEE, 2015, pp. 470–475.

[4] F. Matichard *et al.*, "Seismic isolation of advanced ligo: Review of strategy, instrumentation and performance," *Classical and Quantum Gravity*, vol. 32, no. 18, p. 185003, 2015.

[5] L. Van De Ridder, M. Beijen, W. Hakvoort, J. Van Dijk, J. Lötters, and A. de Boer, "Active vibration isolation feedback control for coriolis mass-flow meters," *Control Engineering Practice*, vol. 33, pp. 76–83, 2014.

[6] C. Chen, Z. Liu, Y. Zhang, and C. Chen, "Modeling and adaptive compensation of unknown multiple frequency vibrations for the stabilization and control of an active isolation system," *IEEE Transactions on Control Systems Technology*, vol. 24, no. 3, pp. 900–911, 2016.

[7] G. Hauge and M. Campbell, "Sensors and control of a space-based six-axis vibration isolation system," *Journal of sound and vibration*, vol. 269, no. 3, pp. 913–931, 2004.

[8] A. Preumont, M. Horodinca, I. Romanescu, B. De Marneffe, M. Avraam, A. Deraemaeker, F. Bossens, and A. Abu Hanieh, "A six-axis single-stage active vibration isolator based on stewart platform," *Journal of sound and vibration*, vol. 300, no. 3, pp. 644–661, 2007.

[9] M. McMickell, T. Kreider, E. Hansen, T. Davis, and M. Gonzalez, "Optical payload isolation using the miniature vibration isolation system (mvis-ii)," in *The 14th International Symposium on: Smart Structures and Materials & Nondestructive Evaluation and Health Monitoring*. International Society for Optics and Photonics, 2007, pp. 652 703–652 703.

[10] T. Söderström, "System identification for the errors-in-variables problem," *Transactions of the Institute of Measurement and Control*, vol. 34, no. 7, pp. 780–792, 2012.

[11] E. Zhang and R. Pintelon, "Errors-in-variables identification of dynamic systems in general cases," *Proc. IFAC Symp. System Identification (SYSID)*, vol. 48, no. 28, pp. 309–313, 2015.

[12] J. Agüero and G. Goodwin, "Identifiability of errors in variables dynamic systems," *Automatica*, vol. 44, no. 2, pp. 371–382, 2008.

[13] R. Pintelon, J. Schoukens, G. Vandersteen, and K. Barbé, "Estimation of nonparametric noise and frf models for multivariable systemspart ii: Extensions, applications," *Mechanical Systems and Signal Processing*, vol. 24, no. 3, pp. 596–616, 2010.

[14] Y. Shin and K. Kim, "Performance enhancement of pneumatic vibration isolation tables in low frequency range by time delay control," *Journal of Sound and Vibration*, vol. 321, no. 3, pp. 537–553, 2009.

[15] D. Tjepkema, "Active hard mount vibration isolation for precision equipment," Ph.D. dissertation, University of Twente, Enschede, The Netherlands, 2012.

[16] M. Tan and J. Hammond, "A non-parametric approach for linear system identification using principal component analysis," *Mechanical Systems and Signal Processing*, vol. 21, no. 4, pp. 1576–1600, 2007.

[17] R. Pintelon and J. Schoukens, *System identification: a frequency domain approach*. John Wiley & Sons, 2012.

[18] T. Oomen, R. van der Maas, C. Rojas, and H. Hjalmarsson, "Iterative data-driven H_∞ norm estimation of multivariable systems with application to robust active vibration isolation," *IEEE Transactions on Control Systems Technology*, vol. 22, no. 6, 2014.

[19] R. Voorhoeve, A. Van Rietschoten, E. Geerardyn, and T. Oomen, "Identification of high-tech motion systems: An active vibration isolation benchmark," *IFAC-PapersOnLine*, vol. 48, no. 28, pp. 1250–1255, 2015.

[20] E. Wernholt and S. Gunnarsson, "Analysis of methods for multivariable frequency response function estimation in closed loop," in *46th IEEE Conference on Decision and Control*. IEEE, 2007, pp. 4881–4888.

[21] Q. Leclère, N. Roozen, and C. Sandier, "On the use of the H_s estimator for the experimental assessment of transmissibility matrices," *Mechanical Systems and Signal Processing*, vol. 43, no. 1, pp. 237–245, 2014.

Appendix A: Bias for H_1 estimator

Recall the expression for $\hat{\mathbf{S}}_{\mathbf{YU}}$ in (20). Substitution of (16) and (19) in (20), and with $M \to \infty$, (20) asymptotically approximates to

$$\begin{aligned}\hat{\mathbf{S}}_{\mathbf{YU}}(\omega) = \mathbb{E}[\boldsymbol{Y_0}(\omega)\boldsymbol{U_0}^H(\omega)] + \mathbb{E}[\boldsymbol{N_Y}(\omega)\boldsymbol{U_0}^H(\omega)] \\ + \mathbb{E}[\boldsymbol{Y_0}(\omega)\boldsymbol{N_U}^H(\omega)] + \mathbb{E}[\boldsymbol{N_Y}(\omega)\boldsymbol{N_U}^H(\omega)].\end{aligned} \tag{26}$$

Under Assumptions 1 and 2, (26) reduces to

$$\hat{\mathbf{S}}_{\mathbf{YU}}(\omega) = \mathbb{E}[\boldsymbol{Y_0}(\omega)\boldsymbol{U_0}^H(\omega)] + \mathbf{C}_{\mathbf{YU}}(\omega). \tag{27}$$

In a similar fashion, an expression for $\hat{\mathbf{S}}_{\mathbf{UU}}$ is obtained,

$$\hat{\mathbf{S}}_{\mathbf{UU}}(\omega) = \mathbb{E}[\boldsymbol{U_0}(\omega)\boldsymbol{U_0}^H(\omega)] + \mathbf{C}_{\mathbf{U}}(\omega). \tag{28}$$

Neglecting leakage effects, and substitution of (26) and (28) in (22), the FRF is estimated as

$$\begin{aligned}\hat{\mathcal{T}}(j\omega) \approx \left(\mathbf{I} + \mathbf{C}_{\mathbf{YU}}(\omega)(\mathbb{E}[\boldsymbol{Y_0}(\omega)\boldsymbol{U_0}^H(\omega)])^{-1}\right)\mathcal{T}(j\omega) \\ \left(\mathbf{I} + \mathbf{C}_{\mathbf{U}}(\omega)(\mathbb{E}[\mathbf{U_0}(\omega)\mathbf{U_0}^H(\omega)])^{-1}\right)^{-1}.\end{aligned} \tag{29}$$